

Origin of magnetic excitation gap in double perovskite $\text{Sr}_2\text{FeOsO}_6$

A. E. Taylor,¹ R. Morrow,^{2,3} M. D. Lumsden,¹ S. Calder,¹ M. H. Upton,⁴ A. I. Kolesnikov,¹ M. B. Stone,¹ R. S. Fishman,⁵ A. Paramakanti,^{6,7} P. M. Woodward,² and A. D. Christianson^{5,1,*}

¹Neutron Scattering Division, Oak Ridge National Laboratory, Oak Ridge, Tennessee 37831, USA

²Department of Chemistry, The Ohio State University, Columbus, Ohio 43210-1185, USA

³Leibniz Institute for Solid State and Materials Research Dresden IFW, Dresden D-01069, Germany

⁴Advanced Photon Source, Argonne National Laboratory, Argonne, Illinois 60439, USA

⁵Materials Science and Technology Division, Oak Ridge National Laboratory, Oak Ridge, Tennessee 37831, USA

⁶Department of Physics, University of Toronto, Toronto, Ontario M5S 1A7, Canada

⁷Canadian Institute for Advanced Research, Toronto, Ontario, M5G 1Z8, Canada

$\text{Sr}_2\text{FeOsO}_6$ is an insulating double perovskite compound which undergoes antiferromagnetic transitions at 140 K (T_{N1}) and 67 K (T_{N2}). To study the underlying electronic and magnetic interactions giving rise to this behavior we have performed inelastic neutron scattering (INS) and resonant inelastic x-ray scattering (RIXS) experiments on polycrystalline samples of $\text{Sr}_2\text{FeOsO}_6$. The INS data reveal that the spectrum of spin excitations remains ungapped below T_{N1} , however below T_{N2} a gap of 6.8 meV develops. The RIXS data reveals splitting of the T_{2g} multiplet consistent with that seen in other $5d^3$ osmium based double perovskites. Together these results suggest that spin-orbit coupling is important for ground state selection in $3d$ - $5d^3$ double perovskite materials.^a

A strong spin-orbit interaction is inherent to $4d$ and $5d$ ions, and when this is manifest in the collective properties of materials via spin-orbit coupling (SOC) it fosters a host of unconventional phases. For example, SOC is responsible for the $J_{\text{eff}} = 1/2$ electronic ground state which leads to a Mott insulating phase in $5d^5$ Sr_2IrO_4 [1], and Kitaev quantum-spin-liquid-like behavior in $4d^5$ RuCl_3 [2]. Beyond this $J_{\text{eff}} = 1/2$ paradigm, however, the influence of the spin-orbit interaction on the electronic ground state and emergent properties in $4d$ and $5d$ transition metal oxides (TMOs) has been poorly understood.

Recently, a SOC-controlled $J = 3/2$ ground state was discovered in $5d^3$ TMOs Ba_2YOsO_6 and $\text{Ca}_3\text{LiOsO}_6$ [3], in contrast with expectations of an orbitally quenched $S = 3/2$ singlet. Ref. 3 revealed a SOC-induced splitting of the t_{2g}^3 manifold via resonant inelastic x-ray scattering (RIXS) measurements, which is driven by strong Os-O hybridization. This confirmed the presence of an unquenched orbital moment in the d^3 ion ground state, and placed these $5d^3$ materials in the intermediate coupling regime, between LS and jj coupling limits. There is therefore immediate interest in exploring the impact of this $J = 3/2$ ground state on the emergent properties in d^3 TMOs.

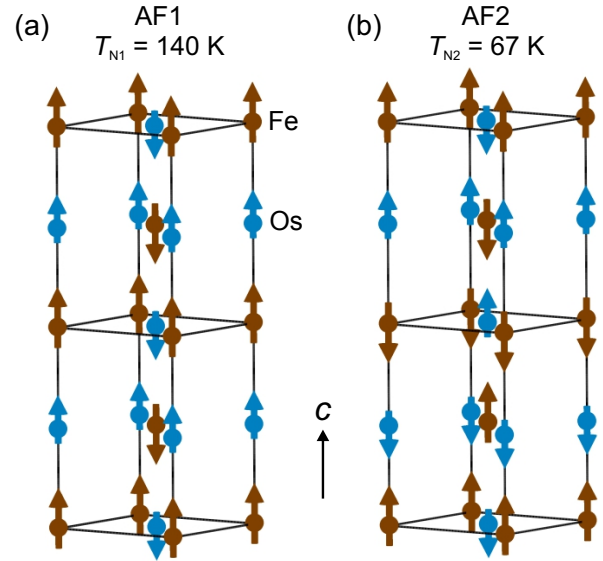


Figure 1. Magnetic structure of $\text{Sr}_2\text{FeOsO}_6$ determined by Refs. 4 and 5. (a) AF1 phase which is dominant between 140 K and 67 K and (b) AF2 phase which emerges at 67 K. The Os (Fe) atoms and direction of the ordered magnetic moment are indicated by the blue (brown) circles and arrows. Two crystallographic unit cells are shown so that the changes between magnetic phases are apparent.

^a This manuscript has been authored by UT-Battelle, LLC under Contract No. DE-AC05-00OR22725 with the U.S. Department of Energy. The United States Government retains and the publisher, by accepting the article for publication, acknowledges that the United States Government retains a non-exclusive, paid-up, irrevocable, world-wide license to publish or reproduce the published form of this manuscript, or allow others to do so, for United States Government purposes. The Department of Energy will provide public access to these results of federally sponsored research in accordance with the DOE Public Access Plan (<http://energy.gov/downloads/doe-public-access-plan>).

In the cubic double perovskite Ba_2YOsO_6 the direct influence of the $J = 3/2$ SOC has been observed via a spin-gap in the magnetic excitation spectrum with inelastic neutron scattering [6]. More broadly, spin gaps have been observed in many single magnetic ion containing $4d^3$ and $5d^3$ double perovskites and related materials [6–11]. These results indicate that SOC directly influences the magnetic ground state in otherwise frustrated systems, which provides scope for control of the physi-

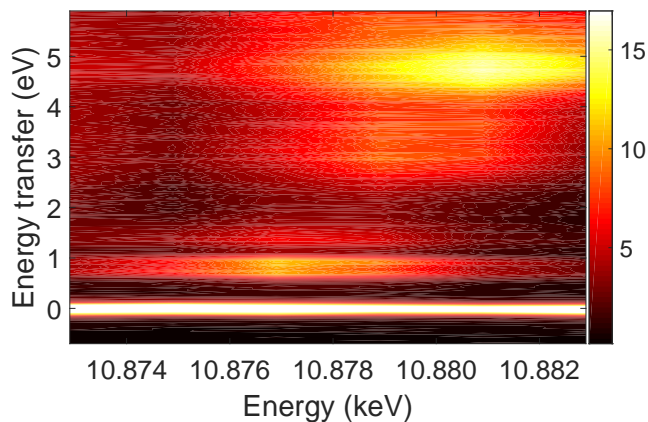


Figure 2. RIXS data showing the incident energy dependence of electronic excitations in $\text{Sr}_2\text{FeOsO}_6$. Measurements were performed at 6 K. The color bar on the right indicates intensity in arbitrary units.

cal properties of such materials via SOC. However, for practical functional materials, the role which SOC plays in significantly non-cubic materials, and in systems with more complex interactions e.g. mixed $3d$ - $5d$ systems, are open questions. Here, we investigate these issues in the $3d$ - $5d$ material $\text{Sr}_2\text{FeOsO}_6$.

$\text{Sr}_2\text{FeOsO}_6$ has attracted a great deal of attention due to highly tunable magnetic behaviour [4, 5, 12–16], and because it is an unusual anomaly in the important series of compounds $\text{Sr}_2BB'\text{O}_6$, where B and B' are $3d$ and $4d$ or $5d$ magnetic transition metal ions, respectively. These materials are well-known for their potential spintronics applications, and they generally present above room-temperature ferrimagnetism and evolve from half-metallic to insulating states as T_C increases: $\text{Sr}_2\text{FeReO}_6$ $T_C = 401$ K, $\text{Sr}_2\text{FeMoO}_6$ $T_C = 420$ K, Sr_2CrWO_6 $T_C = 450$ K, $\text{Sr}_2\text{CrReO}_6$ $T_C = 625$ K, and $\text{Sr}_2\text{CrOsO}_6$ $T_C = 725$ K [17]. However, $\text{Sr}_2\text{FeOsO}_6$ with Os^{5+} ($5d^3$, $S = \frac{3}{2}$) and Fe^{3+} ($3d^5$, $S = \frac{5}{2}$) is an insulating antiferromagnet which undergoes two magnetic transitions at much lower temperatures, $T_1 = 140$ K and $T_2 = 67$ K with Fe and Os ordering in both of the magnetic phases (Fig. 1) [4].

The presence of two transitions in $\text{Sr}_2\text{FeOsO}_6$ suggests competing magnetic interactions. The competition in $\text{Sr}_2\text{FeOsO}_6$ is further demonstrated by the ease with which it can be tuned to other magnetic ground states, either by isoelectronic doping on the A site [13], or via hydrostatic pressure [15], which opens a route to strain-controlled epitaxial films as functional devices [15]. Multiple first principles calculations have attempted to identify the interactions controlling this system, yet have produced disparate results with predictions including semiconductor behavior [18, 19], orbital order [4], dominant Fe-O-Os superexchange interactions [20], or dominant Os-O-O-Os extended superexchange [21]. None of these works considered the potential role of the recently discov-

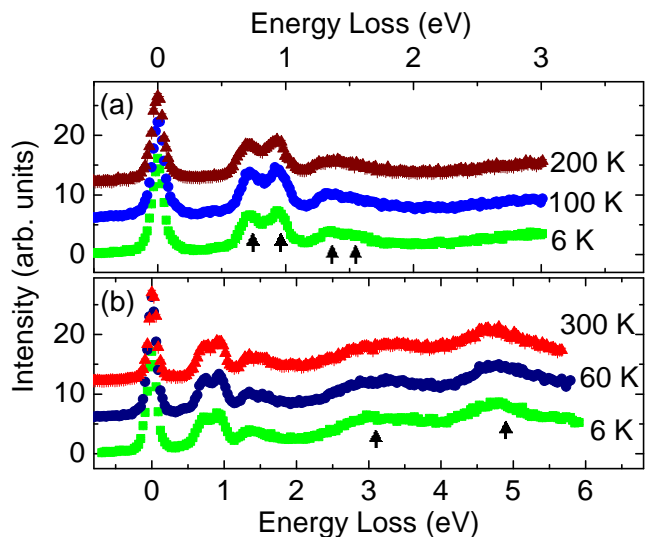


Figure 3. RIXS data from $\text{Sr}_2\text{FeOsO}_6$. (a) High resolution data with $E_i = 10.877$ keV showing excitations (indicated by arrows) within the t_{2g} multiplet. (b) Low resolution RIXS data with $E_i = 10.879$ keV. The arrows indicate the positions of excitations from the t_{2g} to the e_g multiplets. In (a) and (b) an offset of 6 between data sets has been added for clarity.

ered $J = 3/2$ ground state possible for the Os^{5+} ions[3].

Here we experimentally probe $\text{Sr}_2\text{FeOsO}_6$ via inelastic neutron scattering (INS) and resonant inelastic x-ray scattering (RIXS). We find that despite the tetragonal distortion, SOC induced splitting of the Os^{5+} t_{2g} levels is observed, indicative of a $J = 3/2$ ground state. This provides a route to strong entry of SOC in this material - a factor which has not previously been explored - and this conjecture is confirmed, as we reveal a spin-gap in the magnetic excitation spectrum via INS. Previously no such feature has been identified in a $3d$ - $5d$ TMO, only in purely $4d$ or $5d$ materials. Unexpectedly, this SOC-induced gap only emerges below the second magnetic ordering temperature $T_2 = 67$ K. This suggests that SOC is likely intimately linked to the selection of the ground state in $\text{Sr}_2\text{FeOsO}_6$ via SOC-induced anisotropy, similar to Ba_2YOsO_6 and $\text{Sr}_2\text{ScOsO}_6$ [3, 10]. These considerations should also apply to other $3d$ - $5d^3$ combinations such as the high ordering temperature $\text{Sr}_2\text{CrOsO}_6$ [22, 23].

The 12.8 g polycrystalline $\text{Sr}_2\text{FeOsO}_6$ sample was synthesized by combining stoichiometric quantities of SrO_2 , Os , OsO_2 and Fe_2O_3 . Ground mixtures were contained in alumina tubes and sealed in evacuated silica vessels for heatings of 48 hours at 1000°C . This was followed by a regrinding and identical reheating. Laboratory x-ray diffraction measurements were performed to characterize the structural order of the samples studied here. Additional characterization of the structural and magnetic order was provided by neutron powder diffraction measurements performed with HB-2A at the High Flux Isotope Reactor at Oak Ridge National Laboratory (ORNL). The

results of the x-ray and neutron diffraction measurements are given in the supplemental material[24].

Inelastic neutron scattering measurements were performed with the SEQUOIA chopper spectrometer [25] at the Spallation Neutron Source at ORNL. The sample was sealed in a flat plate Al cell with 2 mm thickness in order to minimize the effects of absorption. This cell and an identical empty cell were measured in a closed-cycle refrigerator, accessing temperatures between 5 K and 170 K. Incident neutron energies (E_i s) of 20 and 60 meV, with fermi chopper frequencies of 120 and 180 Hz respectively, were used. Empty-cell background data has been subtracted from all datasets presented.

RIXS spectra were collected on a small portion of the sample on Sector 27 at the Advanced Photon Source (APS) using the MERIX instrumentation [26]. The sample temperature was controlled between 6 K and 300 K in a closed-cycle refrigerator. Primary diamond(1 1 1) and secondary Si(4 0 0) monochromators were used to access the Os L_3 -edge E_i , with a diced Si(4 6 6) analyzer to discriminate the scattered beam energy yielding a energy resolution of 125 meV FWHM. Some scans were also collected with a channel cut Si (4 6 6) analyzer yielding an energy resolution of 55 meV FWHM. A MYTHEN strip detector was used, and experiments were performed in horizontal geometry with $2\theta = 90^\circ$. Data are normalized to the incident beam intensity via an ion chamber monitor.

Figure 2 displays the excitation spectrum of $\text{Sr}_2\text{FeOsO}_6$ measured with RIXS as a function of E_i . As in the case of other osmium-based TMOs[3, 27, 28], the relative energies of the inelastic features along with the dependence of the inelastic features on E_i allows for the identification of intra t_{2g} processes (maximum intensity near 10.877 keV) and $t_{2g} - e_g$ processes (maximum intensity near 10.881 keV).

Figure 3 shows the RIXS spectra from $\text{Sr}_2\text{FeOsO}_6$ measured at selected temperatures in high resolution (a) and low resolution configurations (b). SOC-induced splitting of the t_{2g} character excited state is apparent at all temperatures in the peaks centered around ~ 0.75 eV. Peak splitting around ~ 1.5 eV is not resolved, but the width which is significantly broader than instrumental resolution and the asymmetric shape of the signal indicate that two peaks are likely present, as found in Ba_2YOsO_6 and $\text{Ca}_3\text{LiOsO}_6$ [3]. At present it is not clear why the two peaks are not well resolved. Possibilities include the overall tetragonal symmetry and the antisite mixing with 0.856(4) Fe (Os) and 0.144(4) Os (Fe) occupancy on the B (B') site [24] which is within the typical range for this material [4, 13, 14].

The high resolution RIXS data were fit with a Lorentzian peak shape, giving excited state energies of 0.717(3), 0.936(4), 1.34(7) and 1.5(2) eV at 6 K. This compares with 0.745(7), 0.971(7), 1.447(9) and 1.68(1) eV from Ref. 3 for Ba_2YOsO_6 . As was done in Ref. 3, these

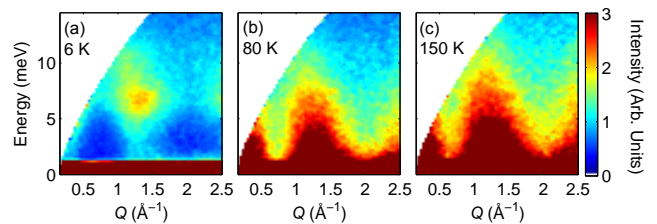


Figure 4. Neutron scattering intensity maps showing the evolution of the scattering from (a) $T = 6$ K ($T < T_{N2}$), (b) $T = 80$ K ($T_{N2} < T < T_{N1}$), (c) $T = 150$ K ($T > T_{N1}$). The incident energy was 20 meV. A gap in the magnetic excitations emerges below T_{N2} as seen in (a).

data can be fit with an intermediate coupling model (under the assumption of cubic crystal field splitting) to extract values of the spin orbit coupling, ζ_{SOC} , and Hund's coupling, J_h . To prevent proliferation of fitting parameters we have fixed the Racah parameter B to the value of 0.0405 eV which was determined by Ref. 29 for $5d^3 \text{Re}^{4+}$. Fixing B to other values over a relatively broad range results in similar values of the Hund's coupling. The model parameters are: The Racah parameters B (fixed), C, the crystal field splitting $10Dq$ (fixed), and the spin-orbit coupling ζ_{SOC} . The results of the fits are insensitive to values of $10Dq$ from 3 to 4.8 eV. The resulting parameters of the fits are: $C = 0.21(1)$ eV and $\zeta_{SOC} = 0.33(7)$ eV. $J_h = 3B+C=0.27(1)$ eV. The values are comparable to those found for Ba_2YOsO_6 and $\text{Ca}_3\text{LiOsO}_6$ [3], other related 5d containing double perovskite systems[30, 31] and for NaOsO_3 [32].

A distinction between the RIXS data for $\text{Sr}_2\text{FeOsO}_6$ and other $5d^3$ systems is that there appears to be two excitations between the t_{2g} and the e_g multiplets. These are found to be at 3.05(3) and 4.85(6) eV (indicated by arrows in Fig. 3(b)). The overall tetragonal symmetry of $\text{Sr}_2\text{FeOsO}_6$ is likely not the reason for the appearance of the two features. At the lowest temperatures the oxygen octahedra surrounding the osmium ions are nearly cubic [13, 14] and both features are observed in the RIXS spectra at all temperatures measured with minimal variation. Another possibility is that the antisite mixing between Fe and Os provides two environments for Os resulting in the two peak structure. A more interesting possibility is that the Hund's coupling on Fe and strong Os-O and O-Fe hybridization for e_g orbital results in a large splitting for spin flip and spin parallel excitations from the t_{2g} to the e_g . Such a scenario might, however, lead to a temperature dependent peak splitting depending on the evolution of magnetic correlations on Fe sites.

An overview of the measured INS spectra from 6, 80 and 150 K is shown in Fig. 4. Whilst there is no significant change in the inelastic spectrum upon crossing T_{N1} , below T_{N2} there is a pronounced change in the excitation spectrum, as a gap opens and the intensity is concen-

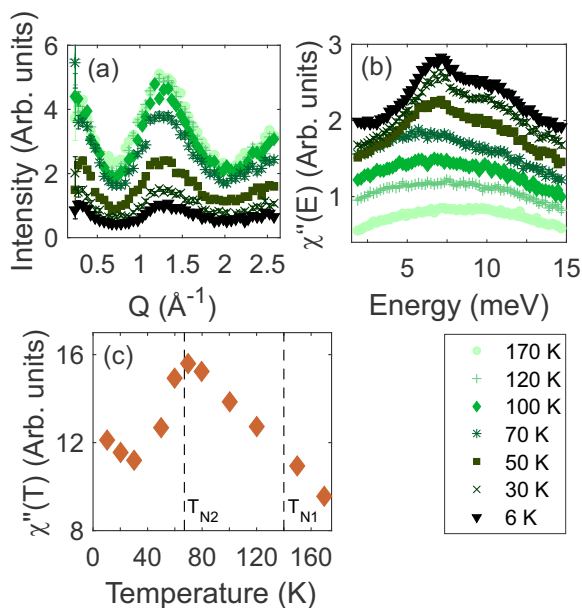


Figure 5. (a) Measured intensity of neutron scattering data averaged over 2–3 meV at temperatures as indicated in the legend in the lower right. (b) Constant-wave vector cuts averaged over 0.8–1.8 Å⁻¹ which have been corrected for the Bose population factor, $1/(1-\exp(-E/k_B T))$. Successive cuts have been offset by 0.2. (c) Data averaged over 2–3 meV and 0.8–1.8 Å⁻¹ and corrected for the Bose factor as a function of temperature, demonstrating temperature dependence of the scattering within the gap. All panels show data collected with $E_i = 20$ meV. In panels (b) and (c) the errorbars are smaller than the symbols.

trated at higher energies, see 6 K data. This behavior is reminiscent of the observed gap development below T_N in the previously measured single-magnetic-ion $4d^3$ and $5d^3$ double perovskites [6–8, 10]. Note that at the lowest temperatures where the spin gap is the strongest the octahedra surrounding the osmium ions are more symmetric [13, 14] than at higher temperatures indicating that a structural distortion at T_{N2} is not likely the origin of the observed spin gap.

The detailed (Q, E) -space temperature dependence of the scattering is presented in Fig. 5. Constant-energy cuts averaged over $2 < E < 3$ meV, i.e. within the gap, are shown in Fig. 5(a). Intensity is observed around wave vector $Q \approx 0.4$ Å⁻¹, which we attribute to scattering near the magnetic wave vector $Q_{AF2} = |(00 \frac{1}{2})| = 0.39$ Å⁻¹. $Q_{AF2} = (00 \frac{1}{2})$ is not an observed magnetic Bragg reflection because the magnetic moments lie along the c axis and only moments perpendicular to Q give neutron scattering intensity. Transverse magnetic fluctuations emerging from $(00 \frac{1}{2})$, however, have a moment perpendicular to Q and can therefore be observed, as in Figs. 4 and 5(a). Therefore the scattering at this purely AF2 wavevector are associated with interactions responsible for the AF2 magnetic order. The $Q \approx 1.3$ Å⁻¹ centered signal in

Figs. 4 and 5(a) is a combination of scattering from $AF1 = (100)$, and $Q_{AF2} = (00 \frac{3}{2})$ and $(10 \frac{1}{2})$ magnetic wave vectors, which cannot be resolved in this measurement. Inspecting Fig. 5(a) it is clear that the fluctuations do not go to zero within the gap at 6 K, which is the result of the presence of a significant fraction (31%) of gapless phase 1 remaining at this temperature (see Fig. S2 and associated discussion [24] and Refs. 4 and 5).

To track the relative strength of the fluctuations with temperature, the data in Fig. 5(b) and (c) have been corrected for the Bose thermal population factor, giving the results in terms of the dynamic susceptibility $\chi''(Q, E)$. The constant-wave vector cuts, averaged over 0.8–1.8 Å⁻¹, in Fig. 5(b) show that there is a significant build up of spectral weight in the range ~ 5 –13 meV below T_{N2} . There is little change in the energy dependence of the scattering at the first transition, $T_{N1} = 140$ K. The onset of the gapped magnetic scattering intensity at low temperature appears to be at $E \approx 5$ meV, and the peak of the intensity is at 6.8(1) meV, determined by fitting two Gaussians on a flat background to the 6 K cut shown in Fig. 5(b). The second peak in intensity is determined to be 10.5(1) meV. The observation of two peaks within the band is consistent with the effects of powder averaging the magnetic excitation signals originating from the inequivalent directions present in the tetragonal crystal structure, as seen in other significantly distorted double perovskites [8]. We compare the peak of the lower band, $\Delta = 6.8(1)$ meV, to previous observations of the gap in $4d^3$ and $5d^3$ double perovskites, as these have followed the convention of using the center of the acoustic band as an estimate of the value of the gap. In Sr₂ScOsO₆, Ba₂YOsO₆, Ba₂YRuO₆ and La₂NaRuO₆ the determined values are $\Delta = 19(2)$ meV, $\Delta = 18(2)$ meV, $\Delta \approx 5$ meV and $\Delta \approx 2.75$ meV, respectively [6–8]. Notably, the energy scale of the gap in Sr₂FeOsO₆ is significantly lower than Os⁵⁺ counterparts Sr₂ScOsO₆ and Ba₂YOsO₆, but still larger than the Ru⁵⁺ examples, in which spin-orbit effects are expected to be reduced.

Another method of estimating the gap was used by Kermarrec *et al.* [6] for Ba₂YOsO₆, in which $\chi''(T)$ for $E < \Delta$ is compared to that expected for a thermally activated excitation, i.e., $\chi''(T < T_{N2}) \propto \exp(-\Delta/k_B T)$. While we see a steep drop in $\chi''(T)$ below T_{N2} in Fig. 5, instead of a plateau above T_{N2} , as seen in Ba₂YOsO₆, the intensity steadily increases with decreasing temperature towards a maximum at T_{N2} . We attribute the steady increase predominantly to the competition between phase 1 and phase 2. Similarly, at very low temperatures $\chi''(T)$ shows a slight upturn, which we attribute to the remaining ungapped AF1 fraction increasingly tending towards AF2 order. Therefore, the temperature dependence in the region $T < T_{N2}$ is not expected to follow a $\exp(-\Delta/k_B T)$ dependence, but instead is a combination of this reduction in intensity with the steadily increasing intensity due to the tendency of the AF1 fraction towards

AF2.

The measurements presented have demonstrated that a SOC-induced gap does emerge in the $3d-5d^3$ system $\text{Sr}_2\text{FeOsO}_6$, but only below the second magnetic transition temperature. The neutron diffraction results show that at all temperatures the AF1 and AF2 magnetic phases are associated with different structural phases[24]. These observations together confirm the notion that the lattice, magnetic and orbital degrees of freedom in this material are all intimately linked. It is worth pointing out that the mixing of Fe and Os sites in this material might be taken to suggest that there are two phases associated with separated Fe-rich and Os-rich regions. However, the constant evolution of the AF1 to AF2 phases below 67 K establishes that there is real competition between these phases not associated with stoichiometry (although local stoichiometry may influence T_{N2}). ^{57}Fe Mössbauer spectroscopy supports this interpretation [5]. Therefore, it appears that SOC is an essential component in selection of the magnetic ground states in $\text{Sr}_2\text{FeOsO}_6$ as was found for $\text{Sr}_2\text{ScOsO}_6$ [10] suggesting that similar considerations are important for understanding the ground states and high ordering temperatures in other $3d-5d^3$ TMOs.

ACKNOWLEDGEMENTS

ADC and RSF were supported by the U.S. Department of Energy, Office of Science, Basic Energy Sciences, Materials Sciences and Engineering Division. RM acknowledges support from the Alexander von Humboldt Foundation. The research at ORNL's Spallation Neutron Source and High Flux Isotope Reactor was supported by the Scientific User Facilities Division, Office of Basic Energy Sciences, U.S. Department of Energy (DOE). Use of the Advanced Photon Source at Argonne National Laboratory was supported by the U. S. Department of Energy, Office of Science, Office of Basic Energy Sciences, under Contract No. DE-AC02-06CH11357. This research was supported in part by the Center for Emergent Materials an National Science Foundation (NSF) Materials Research Science and Engineering Center (DMR-1420451).

* christiansad@ornl.gov

- [1] B. J. Kim, H. Ohsumi, T. Komesu, S. Sakai, T. Morita, H. Takagi, and T. Arima, *Science* **323**, 1329 (2009).
- [2] A. Banerjee, C. A. Bridges, J.-Q. Yan, A. A. Aczel, L. Li, M. B. Stone, G. E. Granroth, M. D. Lumsden, Y. Yiu, J. Knolle, S. Bhattacharjee, D. L. Kovrizhin, R. Moessner, D. A. Tennant, D. G. Mandrus, and S. E. Nagler, *Nat Mater* **15**, 733 (2016).
- [3] A. E. Taylor, S. Calder, R. Morrow, H. L. Feng, M. H. Upton, M. D. Lumsden, K. Yamaura, P. M. Woodward, and A. D. Christianson, *Phys. Rev. Lett.* **118**, 207202 (2017).
- [4] A. K. Paul, M. Reehuis, V. Ksenofontov, B. Yan, A. Hoser, D. M. Többens, P. M. Abdala, P. Adler, M. Jansen, and C. Felser, *Phys. Rev. Lett.* **111**, 167205 (2013).
- [5] P. Adler, V. Ksenofontov, A. K. Paul, M. Reehuis, B. Yan, M. Jansen, and C. Felser, *Hyperfine Interact* **226**, 289 (2013).
- [6] E. Kermarrec, C. A. Marjerrison, C. M. Thompson, D. D. Maharaj, K. Levin, S. Kroecker, G. E. Granroth, R. Flacau, Z. Yamani, J. E. Greedan, and B. D. Gaulin, *Phys. Rev. B* **91**, 075133 (2015).
- [7] J. P. Carlo, J. P. Clancy, K. Fritsch, C. A. Marjerrison, G. E. Granroth, J. E. Greedan, H. A. Dabkowska, and B. D. Gaulin, *Phys. Rev. B* **88**, 024418 (2013).
- [8] A. Aczel, P. Baker, D. Bugaris, J. Yeon, H.-C. zur Loye, T. Guidi, and D. Adroja, *Phys. Rev. Lett.* **112**, 117603 (2014).
- [9] S. M. Disseler, J. W. Lynn, R. F. Jardim, M. S. Torikachvili, and E. Granado, *Phys. Rev. B* **93**, 140407 (2016).
- [10] A. E. Taylor, R. Morrow, R. S. Fishman, S. Calder, A. I. Kolesnikov, M. D. Lumsden, P. M. Woodward, and A. D. Christianson, *Phys. Rev. B* **93**, 220408 (2016).
- [11] S. Calder, D. J. Singh, V. O. Garlea, M. D. Lumsden, Y. G. Shi, K. Yamaura, and A. D. Christianson, *Phys. Rev. B* **96**, 184426 (2017).
- [12] H. L. Feng, M. Arai, Y. Matsushita, Y. Tsujimoto, Y. Guo, C. I. Sathish, X. Wang, Y.-H. Yuan, M. Tanaka, and K. Yamaura, *J. Am. Chem. Soc.* **136**, 3326 (2014).
- [13] R. Morrow, J. W. Freeland, and P. M. Woodward, *Inorg. Chem.* **53**, 7983 (2014).
- [14] A. K. Paul, M. Jansen, B. Yan, C. Felser, M. Reehuis, and P. M. Abdala, *Inorg. Chem.* **52**, 6713 (2013).
- [15] L. S. I. Veiga, G. Fabbris, M. van Veenendaal, N. M. Souza-Neto, H. L. Feng, K. Yamaura, and D. Haskel, *Phys. Rev. B* **91**, 235135 (2015).
- [16] R. C. Williams, F. Xiao, I. O. Thomas, S. J. Clark, T. Lancaster, G. A. Cornish, S. J. Blundell, W. Hayes, A. K. Paul, C. Felser, and M. Jansen, arXiv:1512.04410 [cond-mat] (2015), arXiv: 1512.04410.
- [17] S. Vasala and M. Karppinen, *Progress in Solid State Chemistry* **43**, 1 (2015).
- [18] J. Wang, J. Meng, and Z. Wu, *Chemical Physics Letters* **501**, 324 (2011).
- [19] J. Wang, N. Zu, X. Hao, Y. Xu, Z. Li, Z. Wu, and F. Gao, *Physica Status Solidi (RRL) - Rapid Research Letters* **08**, 776 (2014).
- [20] Y. S. Hou, H. J. Xiang, and X. G. Gong, *Scientific Reports* **5**, 13159 (2015).
- [21] S. Kanungo, B. Yan, M. Jansen, and C. Felser, *Phys. Rev. B* **89**, 214414 (2014).
- [22] Y. Krockenberger, K. Mogare, M. Reehuis, M. Tovar, M. Jansen, G. Vaitheeswaran, V. Kanchana, F. Bultmark, A. Delin, F. Wilhelm, A. Rogalev, A. Winkler, and L. Alff, *Phys. Rev. B* **75**, 020404 (2007).
- [23] R. Morrow, J. R. Soliz, A. J. Hauser, J. C. Gallagher, M. A. Susner, M. D. Sumption, A. A. Aczel, J. Yan, F. Yang, and P. M. Woodward, *Journal of Solid State Chemistry* **238**, 46 (2016).
- [24] See Supplemental Material at [URL will be inserted by publisher] where we discuss additional details regarding the sample characterization..
- [25] M. B. Stone, J. L. Niedziela, D. L. Abernathy, L. DeBeer-Schmitt, G. Ehlers, O. Garlea, G. E. Granroth,

- M. Graves-Brook, A. I. Kolesnikov, A. Podlesnyak, and B. Winn, *Review of Scientific Instruments* **85**, 045113 (2014).
- [26] T. Gog, G. T. Seidler, D. M. Casa, M. H. Upton, J. Kim, S. Stoupin, K. P. Nagle, M. Balasubramanian, R. A. Gordon, T. T. Fister, S. M. Heald, T. Toellner, J. P. Hill, D. S. Coburn, Y.-J. Kim, A. H. Said, E. E. Alp, W. Sturhahn, H. Yavas, C. A. Burns, and H. Sinn, *Synchrotron Radiation News* **22**, 12 (2009).
- [27] S. Calder, J. G. Vale, N. A. Bogdanov, X. Liu, C. Donnerer, M. H. Upton, D. Casa, A. H. Said, M. D. Lumsden, Z. Zhao, J.-Q. Yan, D. Mandrus, S. Nishimoto, J. van den Brink, J. P. Hill, D. F. McMorrow, and A. D. Christianson, *Nat Commun* **7**, 11651 (2016).
- [28] S. Calder, J. G. Vale, N. Bogdanov, C. Donnerer, D. Pincini, M. Moretti Sala, X. Liu, M. H. Upton, D. Casa, Y. G. Shi, Y. Tsujimoto, K. Yamaura, J. P. Hill, J. van den Brink, D. F. McMorrow, and A. D. Christianson, *Phys. Rev. B* **95**, 020413 (2017).
- [29] P. B. Dorain and R. G. Wheeler, *The Journal of Chemical Physics* **45**, 1172 (1966).
- [30] B. Yuan, J. P. Clancy, A. M. Cook, C. M. Thompson, J. Greedan, G. Cao, B. C. Jeon, T. W. Noh, M. H. Upton, D. Casa, T. Gog, A. Paramekanti, and Y.-J. Kim, *Phys. Rev. B* **95**, 235114 (2017).
- [31] A. Paramekanti, D. J. Singh, B. Yuan, Y.-J. Kim, and A. D. Christianson, arxiv.org/abs/1804.02006 (2018).
- [32] J. G. Vale, S. Calder, C. Donnerer, D. Pincini, Y. G. Shi, Y. Tsujimoto, K. Yamaura, M. Moretti Sala, J. van den Brink, A. D. Christianson, and D. F. McMorrow, [arXiv:1707.05551](https://arxiv.org/abs/1707.05551) .